Petroleum Science 20 (2023) 3157–3171

Contents lists available at ScienceDirect

Petroleum Science

journal homepage: www.keaipublishing.com/en/journals/petroleum-science

Original Paper

Characterizations of gas-liquid interface distribution and slug evolution in a vertical pipe

Hai-Yang Yu, Qiang Xu*, Ye-Qi Cao, Bo Huang, Han-Xuan Wang, Lie-Jin Guo**

State Key Laboratory of Multiphase Flow in Power Engineering, Xi'an Jiaotong University, Xi'an, 710049, Shaanxi, China

ARTICLE INFO

Article history:
Received 8 December 2022
Received in revised form
15 March 2023
Accepted 15 March 2023
Available online 16 March 2023

Edited by Jia-Jia Fei

Keywords:
Void fraction
Flow regime
Drift coefficien
Slug frequency
Taylor bubble length

ABSTRACT

Large vertical pipes are key structures connecting subsea wells to offshore platforms. However, existing studies mainly focus on small vertical pipes. In a vertical acrylic pipe with 80 mm inner diameter and 11 m height, a high-speed camera was used to visually research the influences of pipe diameters, liquid properties and inlet effect on air-water co-flow characteristic. Different flow regime maps of vertical pipes (diameters are in the range of 50–189 mm) were compared and the critical gas velocity of the transition boundary from bubble to slug flow tended to increase with the increase of diameters at $D \geq 80$ mm. Drift-flux models were established in different flow regimes and liquid properties have a significant effect on drift coefficients of bubble flow and slug flow (void fraction $\alpha \leq 0.4$). The influence of inlet turbulent effect on the gas-liquid interface distribution gradually weakened and disappeared from the pipe base to 85D, where the flow was fully developed. Slug frequency has a trend of increase first and then decrease with the gas Weber numbers increasing at low liquid superficial velocities ($J_L \leq 0.31$ m/s). And on the basis of this law, a new slug frequency correlation was proposed. It was found that there was an exponential relationship between the ratio of lengths of Taylor bubble to slug and the void fraction.

1. Introduction

The mixture of gas, water and oil is produced from wellheads and transported to offshore platforms through subsea pipelines and vertical pipes (Gao et al., 2020; Xu et al., 2021, 2022; Liu et al., 2021). In large vertical pipes of industrial fields, the strong interaction between gas and liquid causes violent oscillation of pressure and flow rate, which seriously affects safe operation of electric submersible pumps and oil-gas separators (Wang et al., 2018; Hong et al., 2022; Wang Z.N. et al., 2018; Xu et al., 2022). Due to effects of intense pipe wall bondage and bubble swarm wake, existing research conclusions from small vertical pipes are difficult to predict flow parameters (slug frequency and void fraction, etc.) of medium vertical pipes. It is generally accepted that flow data obtained from pipes with diameters larger than 80 mm can be directly used to establish industrial models or to guide the field production (Ali, 2009). Therefore, thoroughly researching the distribution characterizations of gas-liquid interface and the slug evolution mechanism in medium vertical pipes is necessary ($D > 80$ mm).

Flow regimes can intuitively reflect the spatial distribution characteristic between phases and they are the basis for the study of flow parameters (drift velocities and liquid holdup, etc.) in gas-liquid flow (Yin et al., 2018). Flow regime maps were plotted by researchers with methods of the direct observation (high-speed cameras) (Wang T. et al., 2021; Xu et al., 2022) or signals analyzing (differential pressure sensors, conductance probes, etc.) (Abdulkadir et al., 2021; Wang D. et al., 2022) in vertical pipes with different diameters. It is commonly believed that when dimensionless numbers of pipe diameter $D_H^* \geq 40$ ($D_H^* = D_H\sqrt{\sigma/g\Delta\rho}$), Taylor bubbles cannot exist stably (Isao and Mamoru, 1987). D_H, σ, g and $\Delta\rho$ represent the hydraulic diameter, surface tension, gravitational acceleration and density difference of two phases, respectively. Some scholars pointed out (Schlegel et al., 2009) that D_H^* less than 18.6 was the small diameter (corresponding to 50 mm). D_H^* larger than 30 referred to as the large diameter (corresponding to 82 mm) and D_H^* ranging from 18.6 to 30 was called the medium diameter (corresponding to 50–82 mm). In this paper, 100 mm is used as the boundary between the medium diameter and the large diameter (the size data calculated above are applicable to the air-

* Corresponding author.
** Corresponding author.
E-mail addresses: yhy_possible@stu.xjtu.edu.cn (H.-Y. Yu), qiang.xu@mail.xjtu.edu.cn (Q. Xu), lj-guo@mail.xjtu.edu.cn (L.-J. Guo).

https://doi.org/10.1016/j.petsci.2023.03.009

water system) (Wu et al., 2017).

At present, there are abundant researches on flow regime maps in small vertical pipes ($D < 50$ mm) (Taitel et al., 1980; Barnea et al., 1983; Kaji et al., 2009; Szalinski et al., 2010) and large pipes ($D > 100$ mm) (Isao and Mamoru, 1987; Omebere-Iyari et al., 2008; Shoukri et al., 1984; Smith et al., 2012). However, flow regime maps for medium vertical pipes are scarce. Flow regimes in small vertical pipes are strongly bound by the pipe wall (Wang et al., 2017), thus the interphase structure is more stable than that of medium vertical pipes. Large bubbles will deform seriously in large vertical pipes, which makes it difficult to predict the mechanism of interphase action. Flow regime maps of small and large vertical pipes are difficult to be utilized to analyze the flow regime distribution and transition mechanism of medium vertical pipes. Therefore, analyzing flow regime maps is an important part to study the two-phase interface distribution of medium vertical pipes.

In the process of drawing the flow pattern map of the vertical pipe with medium diameter, it is necessary to study the interphase motion mechanism of gas and liquid in order to accurately classify the distribution area and transition boundary of different flow patterns. The drift-flux model including distribution parameter C_0 and drift velocity V_{gj} plays an important role in describing the relative motion trend between phases (Zuber and Findlay, 1965; Isao and Mamoru, 1987; Gui et al., 2019). Nicklin (1962) found that the gas phase drift velocity V_{gj} was $0.35\sqrt{gD}$ when the liquid was stagnant. It has been pointed out that C_0 as well as V_{gj} is influenced by the pipe geometry, pressure and flow direction (Kawanishi et al., 1990). Most drift-flux models are derived from thermodynamic systems with steam-saturated water and their application to the analysis of the C_0 and V_{gj} of conventional vertical pipes with air-water will result in the large deviation. In order to further understand the structural signature and the transition mechanism under diverse flow regimes, it is necessary to study the variation characteristics of parameters in drift-flux models.

As one of the typical flow patterns of two-phase flow, slug flow is commonly found in production pipelines of oil fields with long production life and declining oil and gas production. However it will bring a series of safety hazards to on-site production (Wang Z. et al., 2021; Xie et al., 2019; Xu et al., 2022) including large fluctuation of pressure and aggravation of corrosion in pipes (Xu et al., 2022; Zhang and Lan, 2017), vibration, deformation, breakage and leakage of the whole pipeline, etc. (Gu et al., 2018; Gao et al., 2020; Sekhavati et al., 2022; Wang Y. et al., 2022). Therefore, researching the evolution mechanism of slug flow plays an important role in ensuring production safety. Current researches mainly include slug frequency as well as slug length. Slug frequency is a key parameter to study the erosion and vibration of pipelines. Accurate prediction of slug frequency is an important part of establishing a security defense system for subsea pipelines. The first slug frequency prediction correlation was presented in a 190 mm inner-diameter horizontal pipe (Gregory and Scott, 1969). Hernandez–Perez et al. (2010) proposed an empirical formula for predicting the slug frequency based on experimental data of 38 and 67 mm inclination pipes with angles are 0°–90°. Some scholars suggested a new prediction formula based on previous studies, with an accuracy of 70% (Arabi et al., 2020). According to the report (Rodrigues et al., 2020) that the slug frequency presented lognormal distribution in horizontal pipes. Most slug frequency studies focus on horizontal or slightly inclined pipes. Only a few scholars research the slug frequency in vertical pipes (Abdulkadir et al., 2018) and they ignore the influence of liquid properties on slug frequency and accuracies of proposed prediction correlations is not satisfactory.

The liquid slug is one of the important contents in the research of slug flow in medium pipe and it will block the cross section of pipelines, which may cause the flow stagnation in the pipe or even the oilfield dead well. These will seriously threaten the safe operation of monitoring and measuring apparatus (Ju et al., 2022). Exploring the distribution characteristic of liquid slug length can realize the accurate calculation of the liquid phase accumulation and actual pressure gradient in pipes and it is helpful to construct the system of flow monitoring inside pipelines. Some scholars (Van Hout et al., 2002) found that the stable liquid slug lengths were 8–25D. The report (Naidek et al., 2022) suggested that liquid slug length decreased with the increase of fluid viscosity in horizontal pipes and the average length was about 6D (Baba et al., 2018). Current researches on length of liquid slug are mainly involved in horizontal and slight inclined pipes. However, the evolution mechanism and morphological structure of slug flow in pipes with different angles are very different, thus research conclusions from horizontal pipes cannot be directly applied to vertical pipes. Most scholars pay attention to the liquid slug and the understanding of internal relationship between components of slug unit is still insufficient.

In summary, most studies of the two-phase flow characteristic concentrate on small diameters (4–50 mm) and large diameters (above 100 mm) vertical pipes. There are currently lacks of attention to the spatial and temporal distribution characterization of gas-liquid two phase patterns in medium diameter pipes, which are significantly different from those within vertical pipes with small and large diameters. To improve the flow database of industrial pipes and guide the field production, a visual experimental study on interface distribution of gas-liquid and slug characteristic was carried out in 80 mm medium vertical pipe.

Main contributions in this paper are as follows: (1) A flow regime map of medium vertical pipe approaching to the industrial-scale parameter was drawn. Compared with researches from other scholars, the influence of pipe diameters on transition boundaries of different flow regimes was analyzed. (2) The variation trend of C_0 and V_{gi} in the drift-flux model was investigated under different flow regimes. (3) Based on the gas weber number, a prediction correlation formula for slug frequency with a high accuracy and strong applicability was established. (4) The distribution characteristic of slug structure variation with void fraction in vertical pipes was studied.

2. Experimental facilities

The visualization experiment of gas-liquid flow was completed on a vertical pipe system. The system consists of an acrylic transparent vertical pipe section with 11m height and 80 mm inner diameter, which realizes the observation of flow structure inside the pipe. The gas working medium is air and it is compressed and delivered into a buffer tank by a compressor. The liquid working medium is tap water, which is extracted from an upper storage tank by a centrifugal pump. Air and tap water mixed in a mixer and enter into a vertical pipe and is finally discharged. Air is discharged directly into the atmosphere. The tap water is returned to a storage tank for recycling. Fig. 1 shows the schematic of experiment system.

Two mass flowmeters (ranges are 0–30 kg/h and 0–500 kg/h respectively) are set to measure gas mass flow rate and measurement uncertainties of them are ±0.35%. Two volumetric flowmeters with a range of 0–17 Nm^3/h and 0–70 Nm^3/h respectively are set to measure the liquid volumetric flow rate and measurement uncertainties of them are ±0.75%. Seven differential pressure sensors are arranged at 5D, 20D, 30D, 45D, 70D, 85D and 110D from the bottom of the vertical pipe and all of them has the uncertainty of ±0.0375%. Four pressure sensors are placed at 5D, 45D, 85D, and 135D from the bottom of the vertical pipe and all of them have the uncertainty of ±0.075%. 9253 data acquisition cards (National

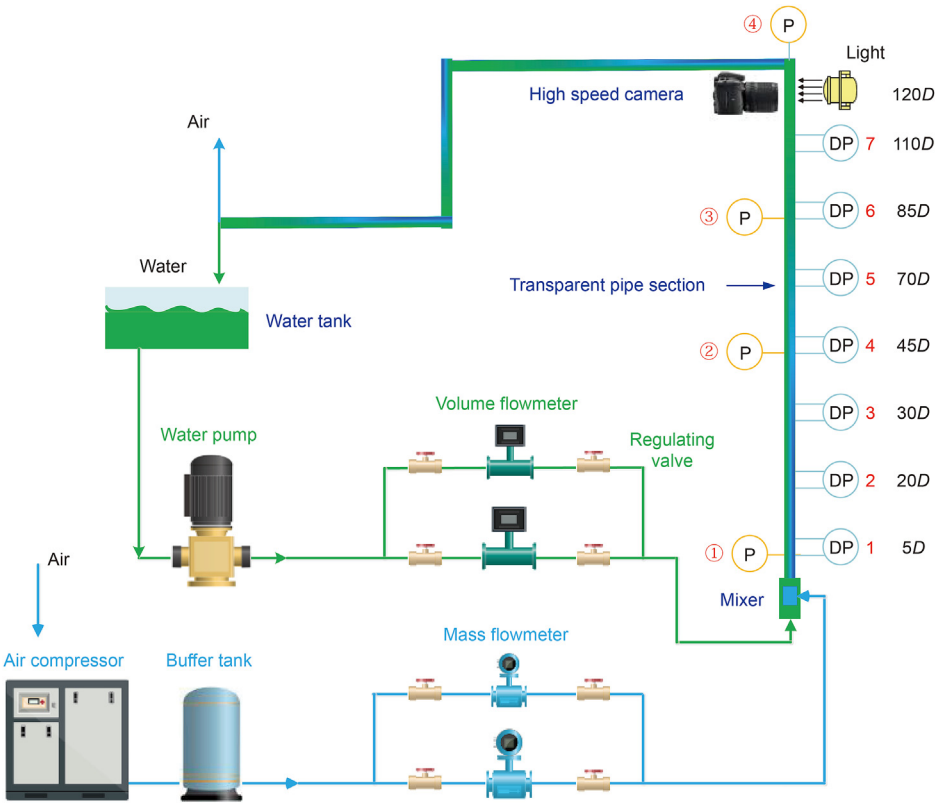

Fig. 1. Schematic of experimental system.

Instrument, USA) are utilized to acquire signals of flowmeters, differential pressure and pressure sensors. The acquisition frequency of all signals in this experiment is 100 Hz, which can accurately obtain real-time flow data in the pipe and the data acquisition time is between 2 and 5 min depending on the flow regime under different working conditions. The resolution and frame rate of the high-speed camera are 1024*512 and 1000 frames/s and which is set up at 120*D* from the vertical pipe base for real-time monitoring the flow status inside the pipe. The gas and liquid superficial velocities are 0.03–16.0 m/s and 0.04–2 m/s respectively and 210 experimental data points were obtained.

3. Data processing and analysis methods

3.1. Measurement of void fraction

Devices for measuring void fraction include the Electrical Capacitance Tomography (ECT), conductivity probes and differential pressure sensors (Gui et al., 2019) and the differential pressure sensor is favored by researchers for their ease of installation and low cost. Total pressure drop consists of the pressure drop of friction, gravity and acceleration in the vertical pipe. The equation is as follows:

$$-\frac{\partial P}{\partial z}=\frac{\tau_0 P}{A}+m^2\frac{d}{dz}\left[\frac{(1-x)^2}{\rho_L(1-\beta)}+\frac{x^2}{\rho_g\beta}\right]+\rho_m g\sin\theta \tag{1}$$

where $-\frac{\partial P}{\partial z}$ and $\frac{\tau_0 P}{A}$ are the total pressure drop and frictional pressure drop, represented by ΔP and ΔP_f, respectively. $m^2\frac{d}{dz}\left[\frac{(1-x)^2}{\rho_L(1-\beta)}+\frac{x^2}{\rho_g\beta}\right]$ is the accelerating pressure drop, accounting for about 2% of the total pressure drop, which can be negligible. $\rho_m g\sin\theta$ is gravity pressure drop, denoted by ΔP_g. ρ_m, ρ_g and ρ_l represent two phases mixture density, gas density and liquid density, respectively. α represents the void fraction. Then the above equation can be transformed into:

$$\Delta P=\Delta P_g+\Delta P_f \tag{2}$$

And void fraction and mixture density can be expressed as:

$$\Delta P_g=\rho_m gh=\left[\rho_g+(1-\alpha)\,\rho_L\right]gh \tag{3}$$

Combining above equation, void fraction α can be obtained by:

$$\alpha=\frac{\Delta P-\Delta P_f-\rho_L gh}{(\rho_g-\rho_L)gh} \tag{4}$$

Eq. (4) shows that void fraction can be obtained by the frictional pressure drop ΔP_f. The frictional pressure drop is negligible when gas-liquid flow rates are small. Under the high gas-liquid flow rates, ΔP_f can be calculated by the separated flow model expressed by the following equations:

$$\Delta P_f=\frac{f_L\rho_L v_L}{2D}\varphi_L^2 \tag{5}$$

$$\varphi_L^2=1+Y+Y^2 \tag{6}$$

where f_L represents the liquid phase friction factor, ρ_L denotes the liquid phase density, v_L denotes the liquid viscosity. φ_L, Y represent the friction factor and the ratio of friction pressure drop between gas and liquid, respectively.

Gas superficial velocity J_G and the gas velocity U_g from image data can be used to calculate the void fraction α and which is taken as the standard value to compare with the α measured by pressure difference sensors. Fig. 2 shows the overall relative deviation of

void fraction α obtained by two methods is within −6%–5%. The result means that differential pressure sensors can measure void fraction α with high accuracy.

3.2. Probability density function (PDF)

The Probability Density Function (PDF) has been proved (Kaji et al., 2009; Abdulkadir et al., 2014) to be a reliable means to identify two-phase flow regimes. For the collected data of a discrete time series, its relative probability density distribution can be obtained by the following equation:

$$\mathrm{PDF}(x_1 < X < x_2) = \int_{x_1}^{x_2} p(x)\mathrm{d}x \tag{7}$$

where x_1 and x_2 are the sizes of statistical intervals and the number of statistical intervals and commonly calculated by adopting the following empirical formula:

$$N = 1.87(n-1)0.4 \tag{8}$$

where, n is the total number of data points, N is the number of statistical intervals, and the size of the statistical interval is:

$$x_2 - x_1 = (p_{\max} - p_{\min})/N \tag{9}$$

PDF can process the timing signal of void fraction and accurately divide the flow regime. Fig. 3 shows signatures of PDF under different conditions. The PDF in bubble flow shows a clear sharp single-peak structure corresponding to a void fraction about 0.25 or less. The PDF of the slug flow has a dual-peak structure. The peak corresponding to high void fraction ε_{TB} represents the large bubble part, while the peak with the low void fraction ε_{gs} represents the portion of liquid slug containing small bubbles. Annular flow also reveals PDF with a single peak structure corresponding to the high void fraction (above 0.8). Churn flow has a single peak with high void fraction and a wide origin at low void fraction, which is the transition regime from slug to annular flow. PDF distribution characteristics of void fraction in each flow regime have obvious differences, which improves the reliability of flow regime division.

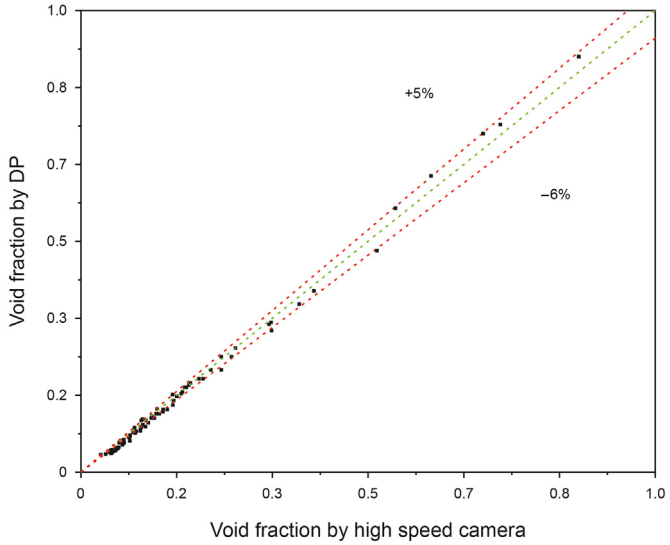

Fig. 2. Void fraction measured by differential pressure sensors and high-speed camera.

3.3. Power Spectrum Density (PSD)

Numbers of slugs passing through the measurement section per unit time is defined as slug frequency, and which can be acquired by the PSD analysis method (Amani et al., 2020). PSD is a probabilistic statistical method. It indicates the distribution characteristic of the signal power with frequency and is the indicator of the mean square value of a random variable.

Fourier transform is applied to random signal sequence $x(n)$ ($n = 0$~$N-1$) to obtain the estimate of PSD directly, as follows:

$$S_x(\omega) = \frac{1}{N}\left|X\left(\mathrm{e}^{j\omega}\right)\right|^2 \tag{10}$$

where $X(\mathrm{e}^{j\omega})$ is the discrete Fourier transform of the signal, and defined as follows:

$$X\left(\mathrm{e}^{j\omega}\right) = \sum_{n=0}^{N-1} x(n)\mathrm{e}^{-j\omega n} \tag{11}$$

The PSD signature of the void fraction sequence signals are performed under different flow conditions in Fig. 4. The PSD of void fraction at different gas superficial velocities (J_G) show the characteristic of the main peak distribution with the highest energy per unit frequency. The frequency and the PSD value of main peaks represent slug frequency and the size of slug unit, respectively. When J_G are above 2 m/s, the transition from slug flow to churn flow occurs and the slug unit no longer exists stably. Therefore, the PSD value of the main peak shows a trend of increase and then decrease with the augment of J_G.

It is also possible to obtain the slug frequency under different flow conditions by image data. The camera is applied to capture the flow data in the pipe for a duration of 11s and the number of slugs that pass during the filming period is artificially counted and recorded. Each group is shot 2–4 times to expand the slug sample to improve the accuracy. And finally, the average slug frequency is obtained.

The manual counting method is taken as the standard and compared with the PSD method, as shown in Fig. 5. Obviously, the slug frequency calculated by PSD has a high accuracy.

4. Results and discussion

4.1. Flow regime map

4.1.1. Comparison of flow regime distribution data from different diameter vertical pipes

Gas-liquid flow regimes in an 80 mm diameter vertical pipe were distinguished as bubble, slug, churn and annular flow under a wide gas and liquid superficial velocity range ($0.03 < J_G < 16$ m/s, $0.04 < J_L < 2$ m/s) by image data and PDF signature of void fraction. Fig. 6(a) and (b) are the flow regime map and show the transition boundaries of different flow regimes derived from published experimental data and models by other scholars. Fig. 6(c) shows the interface structures of gas-liquid two-phase flow in different operating conditions.

Transition from bubble to slug flow in vertical pipes with diameters of 50, 67, 80, 101 and 189 mm were compared. Transition boundaries are similar in 50 mm, 67 mm (Kaji et al., 2009; Szalinski et al., 2010) and 80 mm vertical pipes. However, when the pipe diameters are above 80 mm, the influence of turbulent forces on the gas-liquid interface increases and the bubble-slug flow transition tends to larger gas velocities with the increase of pipe diameters (80 mm, 101 mm (Smith et al., 2012), 189 mm (Omebere-Iyari et al., 2008)).

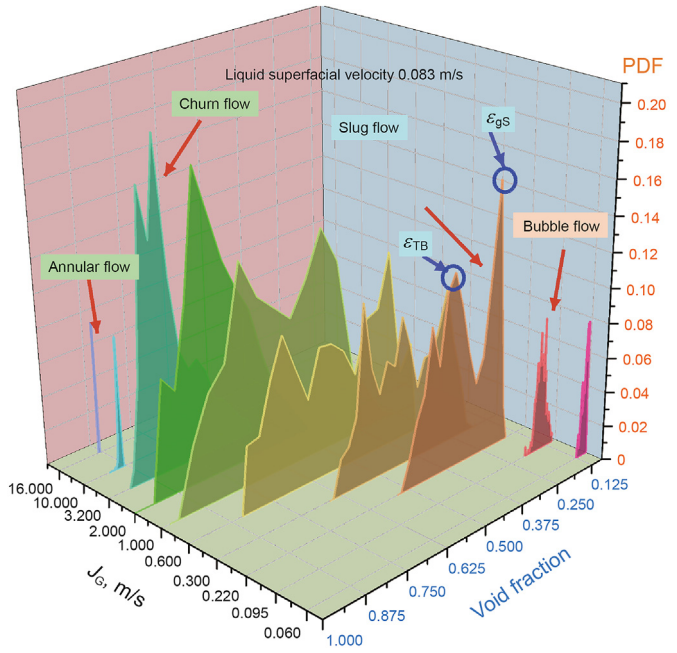

Fig. 3. The PDF of void fraction variation with J_G, at J_L = 0.083 m/s.

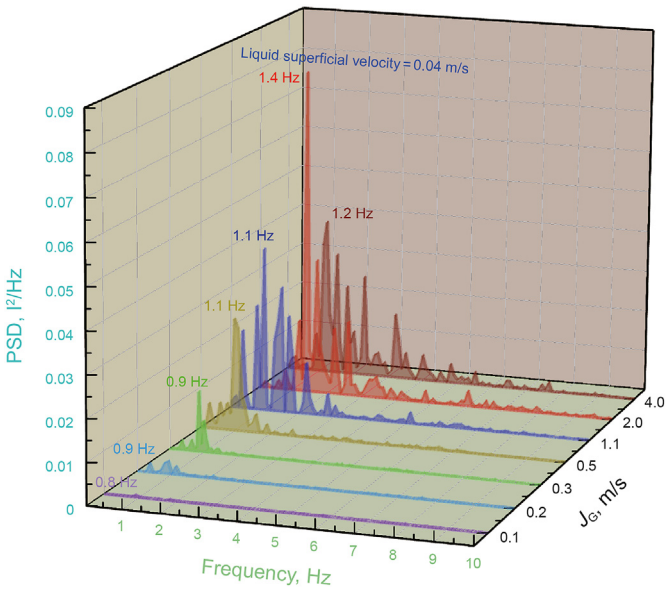

Fig. 4. The PSD signature of void fraction variation with J_G, at J_L = 0.04 m/s.

Slug to churn flow transition boundaries in vertical pipes with diameters of 12.3, 50, 67, 80 and 101 mm were compared. Transition boundaries are similar for vertical pipes of 67 mm (Szalinski et al., 2010) 80 mm and 101 mm (Smith et al., 2012) under the same liquid superficial velocity. It is shown that pipe diameters have little effect on the transition boundary when diameters range from 50 to 100 mm. However, in the range of small diameters (D < 50 mm), increasing the diameter causes destabilization of the gas-liquid interface and large bubbles are more prone to rupture, leading to the transition of flow at lower gas superficial velocities. Thus, the transition boundary in the 50 mm (Kaji et al., 2009) vertical pipe corresponds to smaller gas superficial velocities than 12.3 mm (Barnea et al., 1983) vertical pipe. The same trend was found in other studies (Taitel et al., 1980).

Although cross-sectional sizes of vertical pipes with diameters of 25 mm (Oshinowo and Charles, 1974), 80 mm and 101 mm (Smith et al., 2012) are different significantly, their churn to annular flow transition boundaries corresponding to the similar critical gas superficial velocities. It indicates that pipe diameter has weaker effect on the flow regime transition. The same conclusion was proposed by Taitel et al. (1980) as well. Transition boundaries in different flow regimes are less affected by the pipe diameter at diameters of 50–80 mm through the results of above comparations.

4.1.2. Validation of transition boundary theoretical models

The aggregation and coalescence effect between small bubbles lead to the transition of bubble to slug flow, which generally appears under conditions with small gas superficial velocities (as shown in Fig. 6(c): ((1)–(2), (5)–(6)) and the void fraction (α) in the pipe is 0.25–0.3 (Taitel et al. (1980)). Based on the conclusion from Taitel et al. (1980), Kaichiro and Ishii (1984) proposed a prediction model for the flow transition as shown by black triangular dot line in Fig. 6(b) and the prediction of this model deviates significantly from the present experimental data. The model by Lucas et al. (2005) integrated effects of pipe diameters and observation locations (ratio of length to diameter) on the flow regime transition, which is shown in the Black circle dot line in Fig. 6 (b). Therefore, his model has a high accuracy in predicting the transition boundary of bubble to slug flow for medium vertical pipes.

It is not easily to distinguish Slug to churn flow transition and many scholars propose different mechanistic models to research the transition process (as shown in Fig. 6(c): (6)–(7)), such as the fixed critical void fraction model (Tengesdal et al. (1999)) and the Taylor bubble merger model (Kaichiro and Ishii (1984)). Transition boundaries predicted by models of Tengesdal and Kaichiro show the similar trend to the experimental data, as shown by the square red dot line and the star-shaped black dot line in Fig. 6(b). However, their models are proposed for small vertical pipes and therefore the predicted transition boundaries deviate greatly from present experimental data.

Churn to annular flow indicates that the flow is completely dominated by gas phase (as shown in Fig. 6(c): (4), (8)), at which time almost entire pipe cross-section is occupied by the continuous gas phase and the pressure gradient changes sharply, resulting in

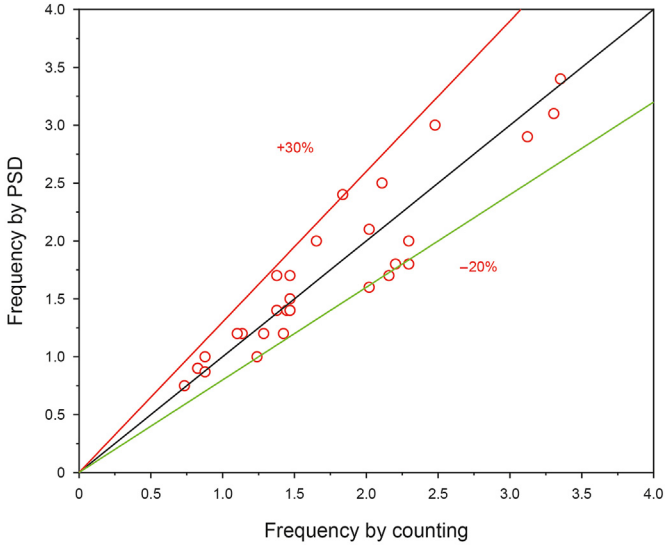

Fig. 5. Slug frequency calculated from the image data and PSD analysis.

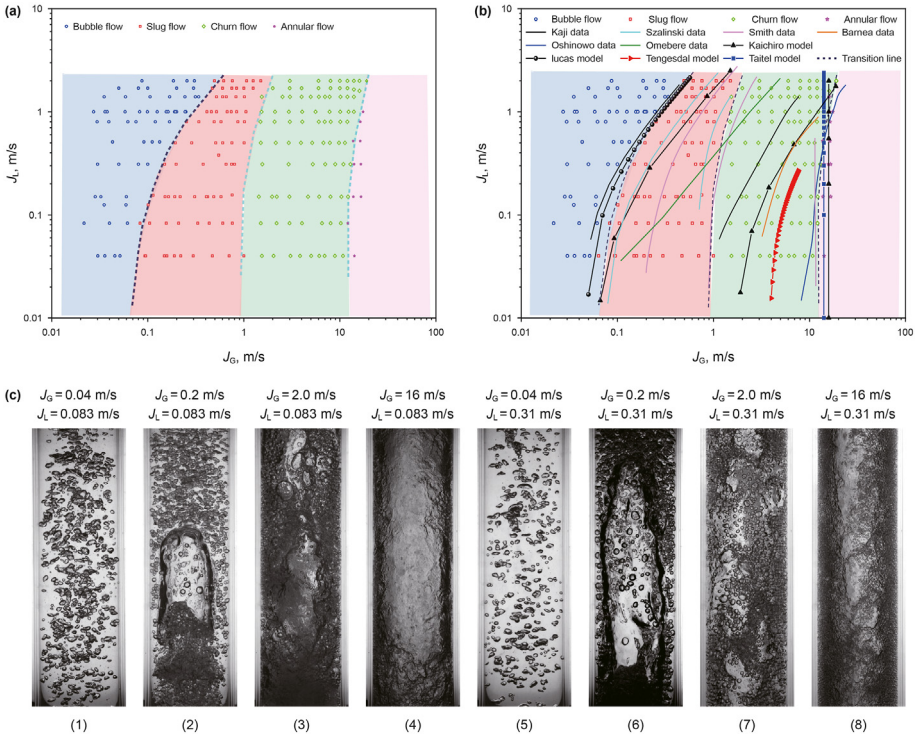

Fig. 6. Flow regime map of a 80 mm diameter vertical pipe (**a**) images and distribution of four flow regimes (**b**) The flow transition boundaries derived from published experiment data and theoretical models by other scholars (Oshinowo and Charles, 1974; Taitel et al., 1980; Barnea et al., 1983; Kaichiro and Ishii, 1984; Tengesdal et al., 1999; Lucas et al., 2005; Omebere-Iyari et al., 2008; Kaji et al., 2009; Szalinski et al., 2010; Smith et al., 2012). (**c**) flow images from high-speed camera in different flow condition.

violent fluctuation of pressure in the pipe and seriously threatening safety production at the site. Therefore, it is important to predict the churn to annular flow transition boundary accurately in the process of oil and gas field extraction. When all the liquid in pipes rise as droplets with the high-speed gas, annular flow happens. The criterion equation for predicting the transition from churn to annular flow (Taitel et al. (1980)) is as follows:

$$U_{GS} = 3.1\left(\frac{\sigma g(\rho_L - \rho_G)}{{\rho_G}^2}\right) \tag{12}$$

where U_{GS}, σ, g, ρ_L, ρ_G denote the actual gas velocity, surface tension, gravitational acceleration, liquid and gas phase density, respectively.

This model by Taitel indicates that parameters such as liquid velocities and pipe diameters don't influence the transition of churn to annular flow, which is only related to the fluid properties, as shown by the square blue dot line in Fig. 6(b).

Kaichiro and Ishii (1984) analyzed the liquid film flow reversal phenomenon around Taylor bubbles and proposed a model for transition from churn to annular flow, as the following equation.

$$U_{GS} = \left(\frac{Dg(\rho_L - \rho_G)}{\rho_G}\right)^{0.5}(\alpha_{sb} - 0.11) \tag{13}$$

$$\alpha_{sb} = 1 - 0.813 \times \left[\frac{(C_0 - 1)u_M + 0.35\sqrt{\frac{Dg(\rho_L - \rho_G)}{\rho_L}}}{u_M + 0.75\sqrt{\frac{Dg(\rho_L - \rho_G)}{\rho_L}}\left(\frac{\rho_L D^3(\rho_L - \rho_G)}{\mu_L^2}\right)^{1/18}}\right]^{0.75} \tag{14}$$

where α_{sb}, D, u_M, μ, C_0. are the void fraction within Taylor bubbles, pipe diameter, two-phase mixing velocity, viscosity and gas phase distribution parameter. This model takes into account the pipe diameter and the critical void fraction in Taylor bubble region and which is plotted with the triangular black dot line in Fig. 6(b). Transition boundaries predicted by models of Kaichiro and Taitel are close to the experimental data.

A large number of experimental data from different pipes were obtained and many scholars have established prediction models for

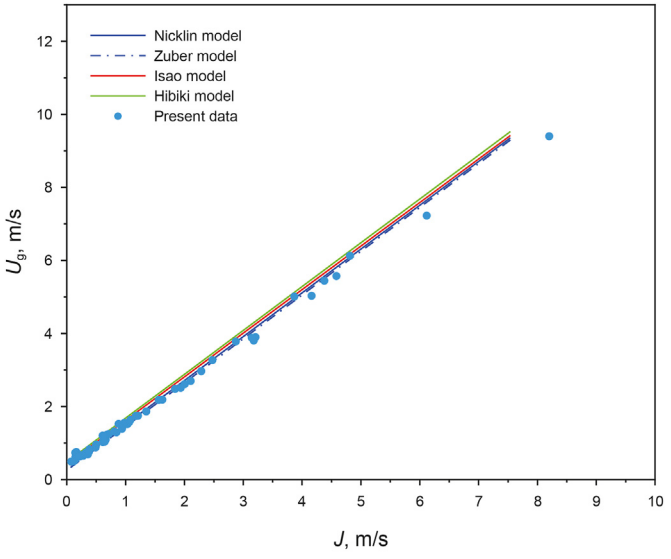

Fig. 7. Drift-flux models from different authors (Nicklin, 1962; Zuber and Findlay, 1965; Isao and Mamoru, 1987; Hibiki and Ishii, 2003).

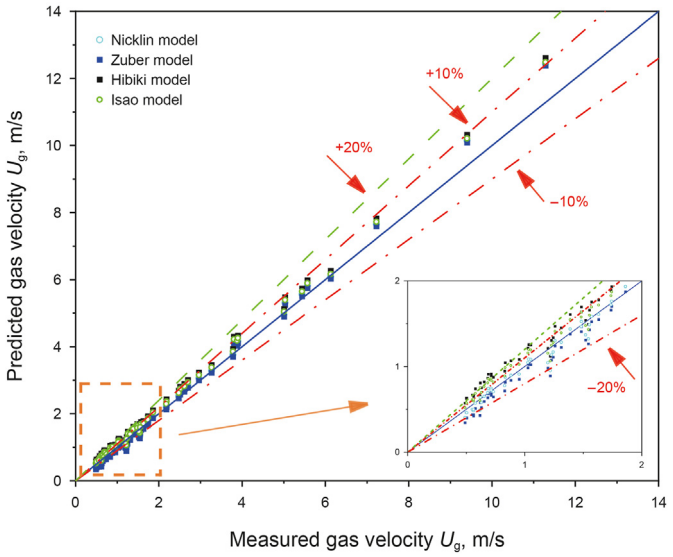

Fig. 8. U_g from drift-flux models and the experiment (Nicklin, 1962; Zuber and Findlay, 1965; Isao and Mamoru, 1987; Hibiki and Ishii, 2003).

a variety of transitions of typical flow regimes. Above comparisons show that when diameters range from 50 to 80 mm, models of Lucas, Kaichiro and Taitel have higher accuracy in predicting transition of bubble to slug flow and churn to annular flow, respectively. However, models of Tengesdal and Kaichiro deviate significantly from the present experimental data in predicting the transition of the slug to churn flow.

4.2. Drift-flux model

The drift-flux model characterizes the constitutive relationship of two-phase flow and it is usually applied to calculate the relative velocity between phases, Zuber and Findlay (1965) first proposed the model and the equations are as follows.

$$U_g = \frac{J_G}{\alpha} = C_0 J + V_{gi} \tag{15}$$

$$C_0 = \frac{\langle \alpha J \rangle}{\langle \alpha \rangle \langle J \rangle} \tag{16}$$

$$V_{gi} = \frac{\langle \alpha v_{gi} \rangle}{\langle \alpha \rangle} \tag{17}$$

$$v_{gi} = v_g - J \tag{18}$$

where U_g, J_G, α and J represent the gas velocity, gas superficial velocity, void fraction and mixture velocity, respectively. v_g and v_{gi} are the local gas phase velocity and local drift velocity. C_0, V_{gi} are the

Table 1
Mean Ralative Error (MRE) of the gas velocity from the experiment and different models.

Model	MRE, %		
	U_g < 2, m/s	U_g > 2, m/s	Overall deviation
Nicklin (1962)	8.5	7.63	7.5
Zuber (1965)	15.2	10.74	12.27
Hibiki (2003)	14.8	10.34	11.53
Isao (1987)	10.6	8.08	9.71

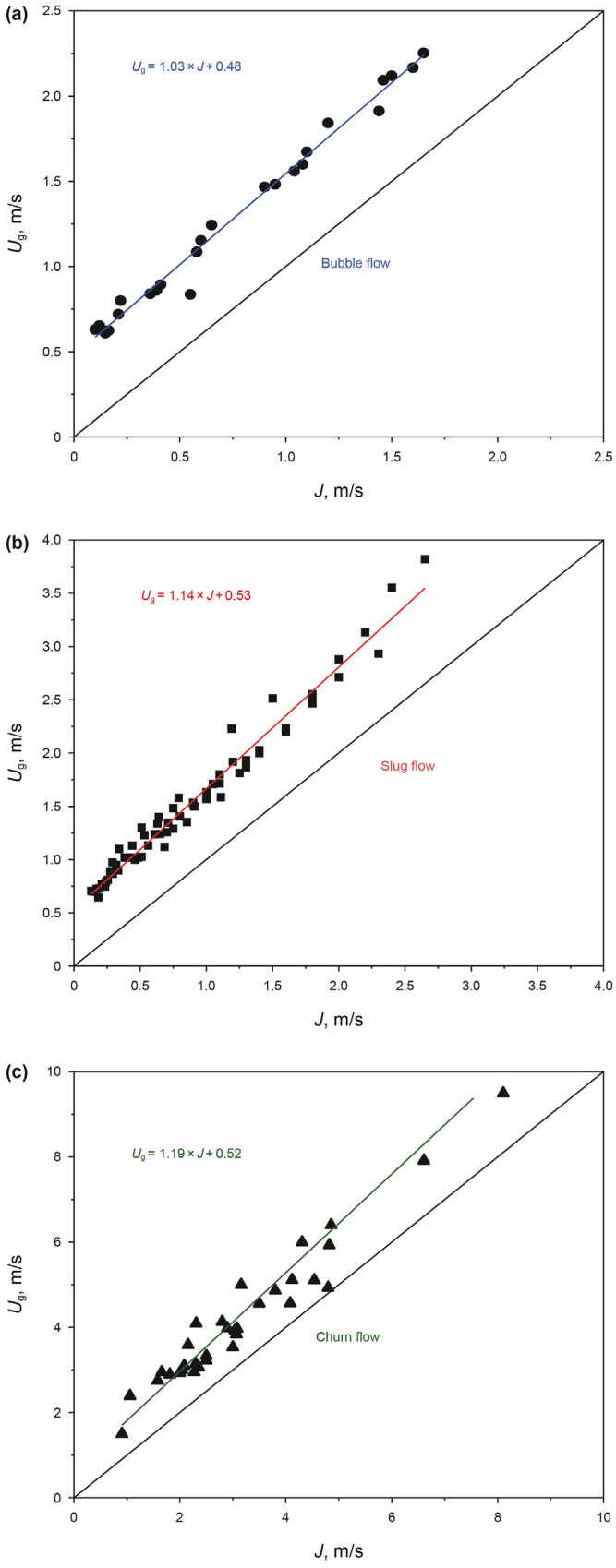

Fig. 9. Drift-flux models fitting under different flow regimes (**a**) Bubble flow (**b**) Slug flow (**c**) Churn flow.

distribution parameter and the average drift velocity, respectively. Drift-flux model takes into account the slip tendency in different phases.

4.2.1. Verification of existing drift-flux models

Eq. (15) shows that the linearity relation between mixture velocity J and the gas velocity U_g. The slope represents C_0 and the intercept represents the V_{gi} of gas when liquid is stagnant. According to drift-flux models from different scholars (Nicklin, 1962; Zuber and Findlay, 1965; Isao and Mamoru, 1987; Hibiki and Ishii, 2003), prediction curves and present experimental data were plotted in Fig. 7. U_g predicted by different models were further compared with that of the experiment, as shown in Fig. 8.

Models of Hibiki and Isao were based on the phenomenon of large vertical pipes, the horizontal disturbance of bubbles inside the pipe will worsen the inhomogeneity distribution of two-phase, resulting in a larger U_g predicted than that of the medium vertical pipe. At $U_g < 2$ m/s, U_g predicted by models of Zuber and Nicklin are lower than U_g from present experiment. However, the result is reversed at $U_g > 2$ m/s. Their models were established based on the study of small vertical pipes, which did not take into consideration the effect of the flow regime transition on C_0 and the V_{gi}, resulting in less accurate prediction for U_g of present experiment.

The relative deviation range of the U_g from present experiment data and U_g from drift-flux models are −20% to +20%. In order to clarify the accuracy of drift-flux models from different scholars, U_g equaling to 2 m/s is taken as the boundary and the Mean Relative Error (MRE) of U_g for experiments and different models is shown in Table 1 below. MRE is large when U_g is less than 2 m/s and which is small when U_g is larger than 2 m/s. The result indicates that at lower gas velocities ($U_g < 2$ m/s), drift-flux models proposed by predecessors have low accuracy in predicting U_g of medium vertical pipes.

Due to flow regimes affecting the distribution of C_0 and V_{gi}, drift-flux models proposed by above scholars have large deviation in predicting the data of medium vertical pipes. Therefore, it is necessary to investigate C_0 and V_{gi} under different flow regimes.

4.2.2. Distribution parameter and drift velocity

Based on the experimental data, drift-flux models are fitted respectively in bubble, slug and churn flow and the correlation between J and U_g are plotted, as shown in Fig. 9. Corresponding distribution parameters C_0 in the region of bubble, slug and churn flow are 1.03, 1.14 and 1.19 respectively and the drift velocities V_{gi} are 0.48, 0.53 and 0.52 m/s, respectively. To facilitate comparison with other studies, the drift velocity is replaced by the drift coefficient using $k = \frac{V_{gi}}{\sqrt{gD}}$ and k denotes the drift coefficient, thus the calculated k values are 0.54, 0.6, and 0.59, respectively. In the study of vertical pipes with diameters greater than 50 mm (Kawanishi et al., 1990), the drift coefficient k (0.52) is close to that in this work.

Fig. 10 shows C_0 and the drift coefficient k in 67 and 80 mm vertical pipes (Abdulkadir et al., 2018). The pipe wall effect in the medium vertical pipe has less influence on the bubbles rising process in bubble flow region so the distribution of bubbles is more uniform and $C_0 \approx 1$, as shown in Fig. 10(a). The aggregation process of small bubbles is promoted with void fraction becoming larger, which makes the flow transit to slug flow and $C_0 \approx 1.14$. When void fraction further increases, the liquid is torn by gas and at this time the churn flow or even annular flow appears, which triggers the instability of flow interface so C_0 reaches about 1.2. The distribution parameters of this experiment are between 1 and 1.2 and similar to the results of current studies. The pipe used in Abdulkadir's experiment is 67 mm and the liquid working medium is silicone oil, therefore his distribution parameter C_0 has significant difference with that of present work under different flow regimes.

In the bubble flow region of Fig. 10(b), the drift coefficient k of the experiment is greater than that of Abdulkadir but the magnitude of both drift coefficients is opposite in slug flow. This manifests that liquid properties have greater effect on k in the regions of bubble flow and slug flow, there are other studies also reporting the same conclusions (Abdulkadir et al., 2014). In churn flow, gas and liquid are fully mixed and the relative velocity difference between phases decreases. Therefore, k in this paper is similar to that of Abdulkadir, at this time, liquid properties don't affect the distribution of drift velocities.

4.3. Influence of inlet effect on flow distribution

There is existing strong gas-liquid turbulence effect at the entrance of vertical pipes, which will cause drastic fluctuation of flow rate and pressure and affect the development of flow in pipes. At present, there is still no consensus on the influence of inlet effect on flow in pipe. It is generally believed that the flow develops stably at 60D from the inlet (Tas-Koehler et al., 2022). However, it is also reported that the length of flow development will reach more than 600 D in some working conditions. Most scholars conduct experimental studies at small range of velocities, resulting in their failure to observe the effect of turbulence on the interface distribution at the entrance under high gas and liquid velocities. Therefore, there is a missing of the comparative analysis about the flow distribution at different locations of pipes.

The distribution of void fraction at different positions ($L = 5D$, $20D$, $30D$, $45D$, $70D$, $85D$, $110D$) of the vertical pipe was plotted under different gas superficial velocities as shown in Fig. 11. The void fraction increases with the increase of J_G at the same position

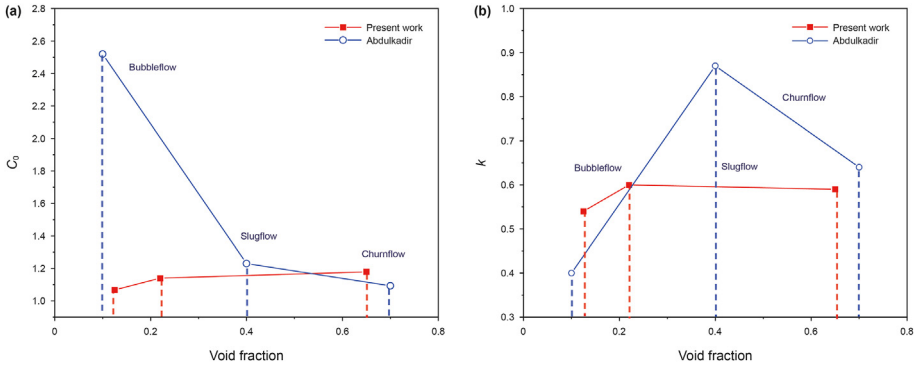

Fig. 10. The variation trends of distribution coefficient C_0 and drift parameter k under different flow regimes, data from present work and Abdulkadir et al., (2018).

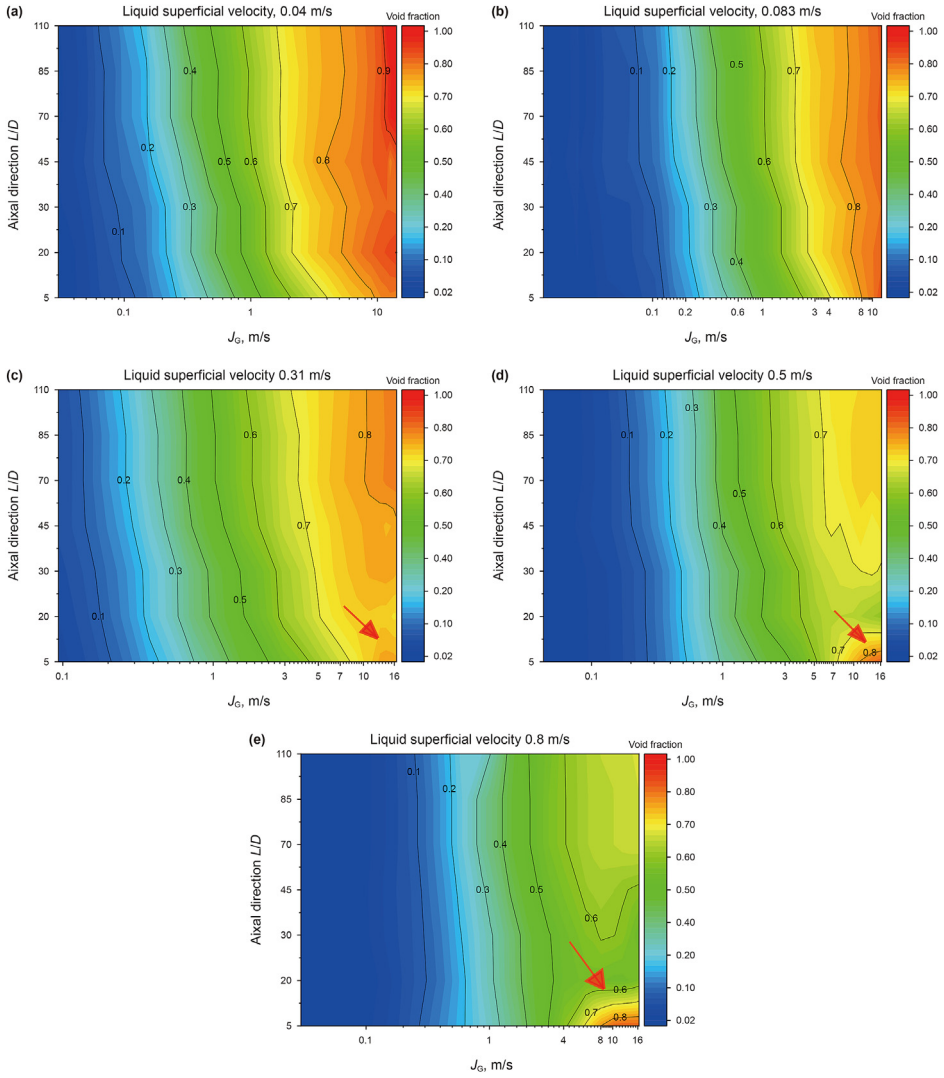

Fig. 11. The distribution diagram of void fraction variation with gas superficial velocity at different positions, J_L, m/s= (**a**) 0.04 (**b**) 0.083 (**c**) 0.31 (**d**) 0.5 (**e**) 0.8.

and also increases with the observation position farther from the inlet under the same gas superficial velocity, as shown in Fig. 11(a) and (b). At about 85*D* from the pipe base, void fraction no longer increases significantly and it can be considered that the flow is fully developed. In Fig. 11(c), (d) and (e), when J_G is greater than 10 m/s, gas will rapidly entrain the liquid and there is forming a flow structure similar to the annular flow at entrance. At this time the turbulence effect is significant, leading to the void fraction near the inlet position (around 5*D*) rapidly increased, as shown by the arrows. The liquid here will be lifted by the gas and not fall back. At 20*D* from the bottom of pipe, the gas lifting is weakened and the gas and liquid are constantly agitated, resulting in the void fraction becoming smaller. After this position, with the increase of *L*/*D*, the void fraction increases again and the turbulent effect at the inlet no longer impacts the downstream flow.

Fig. 12 shows the schematic diagram of gas lifting phenomenon.When J_L are 0.31, 0.5 and 0.8 m/s, the initial gas superficial velocities that cause the significant increase in void fraction at the inlet are 11, 8 and 5 m/s, respectively, as shown by arrows in Fig. 11(c), (d) and (e). It indicates that the influence range of inlet effect gradually spreads to smaller gas velocities with liquid velocity increasing.

Kaji et al. (2009) also found the influence of inlet effect on the

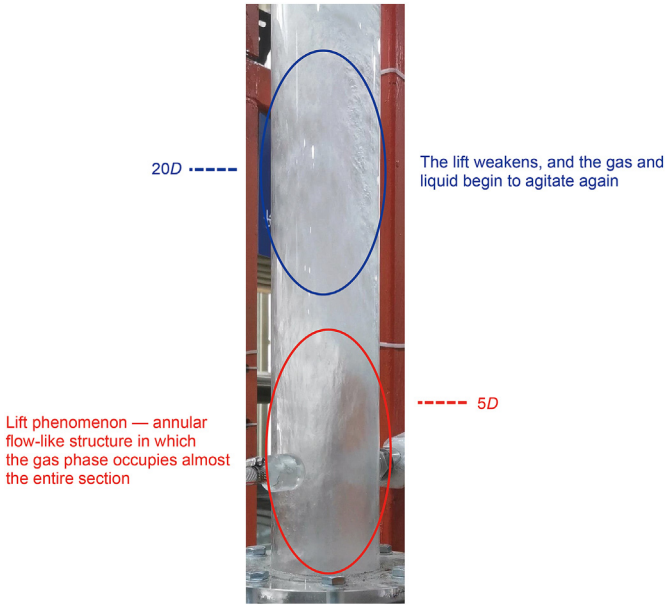

Fig. 12. Actual image of the gas lifting phenomenon at the pipe entrance.

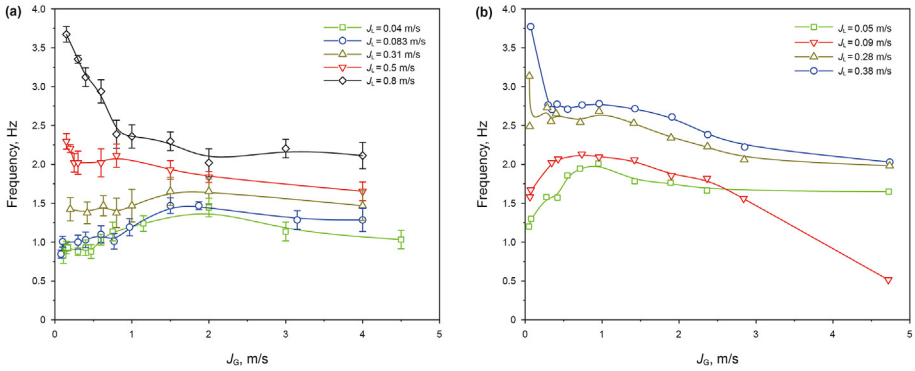

Fig. 13. Variation of slug frequency with J_G under different J_L, (**a**) present work (**b**) Abdulkadir et al., (2018).

flow at a low J_G (0.22 m/s) in a small pipe (50 mm). However, there are no similar phenomenon of the inlet effect at higher gas velocities due to the low gas velocities (less than 0.53 m/s), single J_L (1 m/s) and low vertical pipe height ($H = 68D$) in his experiment.

4.4. Slug frequency

4.4.1. The distribution of slug frequency

Curves of slug frequency variation with J_G were plotted under different liquid superficial velocities, as shown in Fig. 13(a). Under the same gas superficial velocity, increasing J_L will cause liquid to block the pipe section frequently, which leads to a rising trend of slug frequency. Increasing J_G will lead to the increase of slug move velocity and slug length. When J_L and J_G are less than 0.31 and 0.2 m/s, the increasing speed of slug velocity is close to that of slug length and therefore slug frequency has little variation with the augment of J_G. When J_G is greater than 0.2 m/s, the flow region is stable slug flow, in which the growth rate of the slug moving velocity is greater than that of the slug length. Thus, the slug frequency tends to increase as J_G increases. When J_G reaches about 1.5 m/s, the slug flow in the pipe turns to churn flow. At this time, the liquid is destroyed due to the gas bubbles merging process. Since the growth rate of slug moving velocity is less than that of slug length and slug frequency tends to descend with the increase of J_G. When J_L is above 0.31 m/s, liquid phase will promote the merging process of large bubbles in the pipe, which leads to the growth rate of slug moving velocity always less than that of slug length, so slug frequency shows a decreasing trend with gas superficial velocity increasing.

In a vertical pipe (Abdulkadir et al., 2018) with a diameter of 67 mm, the variation of slug frequency is similar to that in this paper, as shown in Fig. 13(b).

Comparing Fig. 13(a) and (b), slug frequency of Abdulkadir experiment is significantly higher than that of present experiment at similar liquid superficial velocities. At $J_L \leq 0.31$ m/s, both experiments observe the existence of maximum slug frequency and

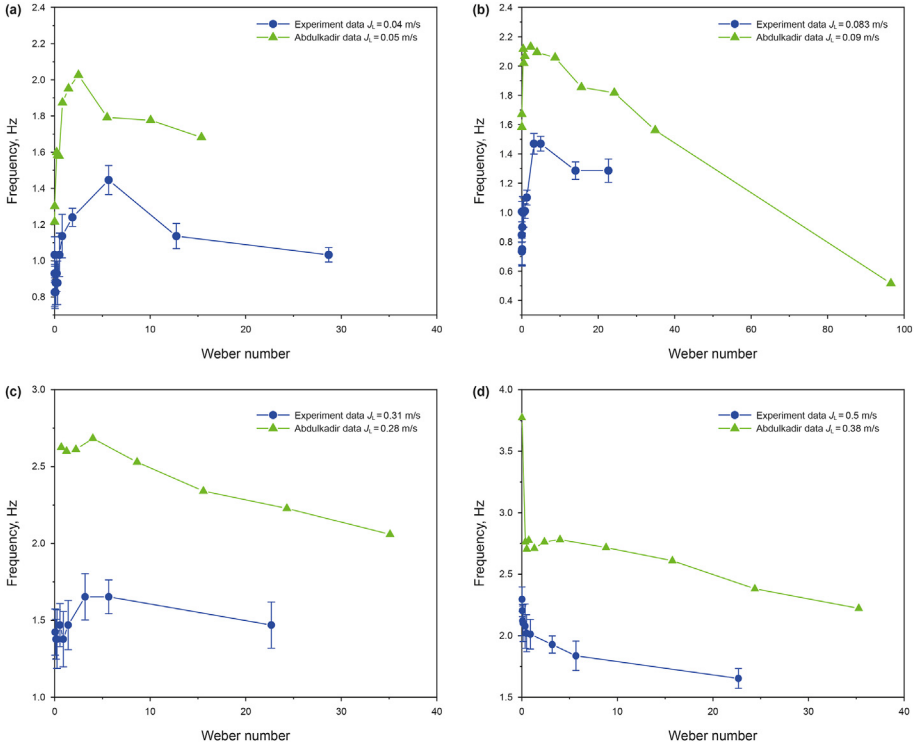

Fig. 14. Slug frequency versus Weber number, data from the experiment and Abdulkadir et al., (2018).

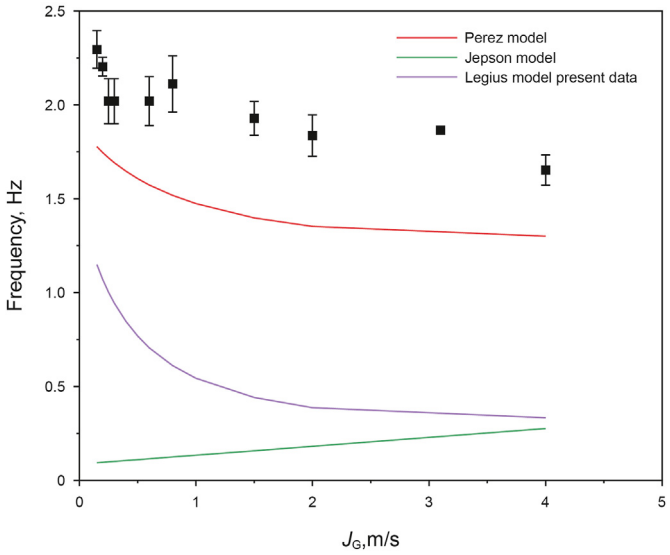

Fig. 15. Distribution of slug frequency from present data and correlations by predecessors (Jepson and Taylor, 1993; Legius et al., 1997; Perez et al., 2010), $J_L = 0.5$ m/s.

the corresponding J_G are 1.5 and 1 m/s, respectively. To explore the slug frequency distribution characteristic, dimensionless Weber number (W_E) is introduced as follows:

$$W_E = \rho_G J_G^2 D \Big/ \sigma \tag{19}$$

W_E denotes the ratio of inertial force to surface tension. Fig. 14(a), (b) and (c) shows that slug frequency increases first and decreases as follow when W_E increases. When W_E is about 5, a maximum slug frequency exists in present work and Abdulkadir's experiment. It means that the dimensionless number W_E plays an important role in analyzing slug frequency distribution under different fluid properties. This finding provides ideas for the establishment of prediction correlations of slug frequency.

4.4.2. Prediction correlation

Fig. 15 shows that slug frequency from the present experimental data and prediction correlations of predecessors (Jepson and Taylor, 1993; Legius et al., 1997; Hernandez–Perez et al., 2010). Researches of Jepon and Legius focus on horizontal or slightly inclined pipe sections so the slug frequency trends predicted by their correlations are significantly different from that in this paper. A correlation from Hernandez-Perez is constructed on experimental pipe sections with inclination angles from 0 to 90°, so the predicted variation trend of slug frequency is similar to that of the experimental data. However, the prediction accuracy is still unsatisfactory.

In summary, based on Hernandez-Perez's research, a new prediction correlation for slug frequency of the medium vertical pipe is proposed as follows.

$$f_s = 0.7\frac{J_L^{0.25}}{R_{eL}^{0.2}} + 0.1W_E \tag{20}$$

for $W_E \le 5, J_L \le 0.31$ m/s

$$f_s = 0.7\frac{J_L^{0.25}}{R_{eL}^{0.2}} - 0.015W_E \tag{21}$$

for $W_E > 5, J_L \le 0.31$ m/s

$$f_s = 0.6\frac{\mu}{\rho D}\left(J_L \Big/ gD\left(\frac{19.75}{J} + J\right)\right)^{0.25} \tag{22}$$

$J_L > 0.31$ m/s.

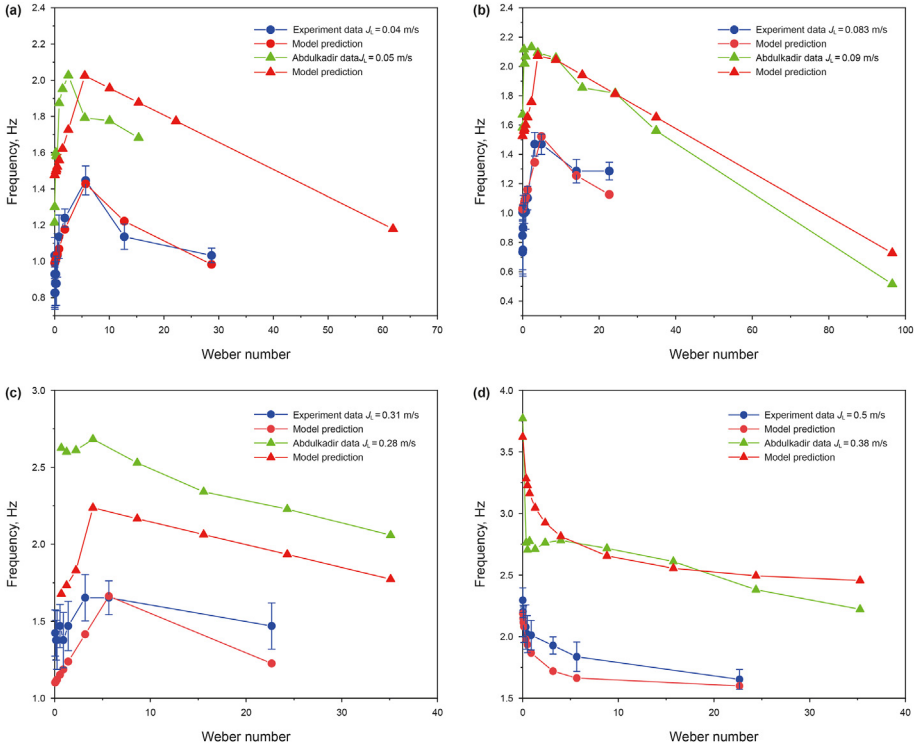

Fig. 16. Comparison of slug frequency of prediction correlations and experiment (data from the experiment and Abdulkadir et al., 2018).

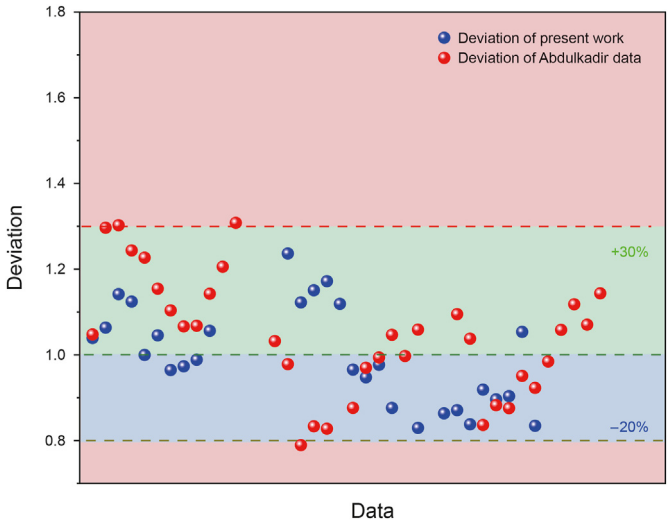

Fig. 17. Deviation between correlation and the data of present work and Abdulkadir et al., (2018).

where R_{eL} is the liquid Reynolds number.

The comparisons of slug frequency from the new correlation with that measured in experiment are plotted in Figs. 16 and 17. Deviations between the calculated and experimental slug frequency are in the range of −20%–30%.

Most of correlations for predicting slug frequency established by predecessors only consider the liquid velocity. The new correlation established in this paper takes into account influences of liquid properties and gas velocities on the distribution of slug frequency. Thereby, it has stronger applicability and can provide guidance for researching slug frequency within medium vertical pipes.

4.5. Slug unit structure

4.5.1. Taylor bubble, liquid slug and slug unit length

A slug unit is the basic structure of slug flow which consists of a Taylor bubble and a liquid slug. In this paper, the lengths of Taylor bubble, liquid slug and slug unit under different working conditions are calculated by image data. The slug unit length is determined by Taylor bubble velocity and slug frequency, as follows:

$$L_{SU} = \frac{U_N}{t_N} \tag{23}$$

$$L_{TB} = \frac{U_{TB}}{t_{TB}} \tag{24}$$

$$L_S = \frac{U_S}{t_S} \tag{25}$$

$$t_N = t_{TB} + t_S = 1/f \tag{26}$$

where, L_{SU}, L_{TB} and L_S are the length of slug unit, Taylor bubble and liquid slug, respectively. U_N, U_{TB} and U_S are the velocity of slug unit, Taylor bubble and liquid slug, respectively. t_N, t_{TB} and t_S represent the time interval of the slug unit, Taylor bubble and liquid slug passing through the observation position, respectively. f represents slug unit numbers passing through the observation position in a unit time. Assuming that each slug unit is fully developed, namely, the head and tail of a slug unit have the same speed, then:

$$U_N = U_{TB} = U_S \tag{27}$$

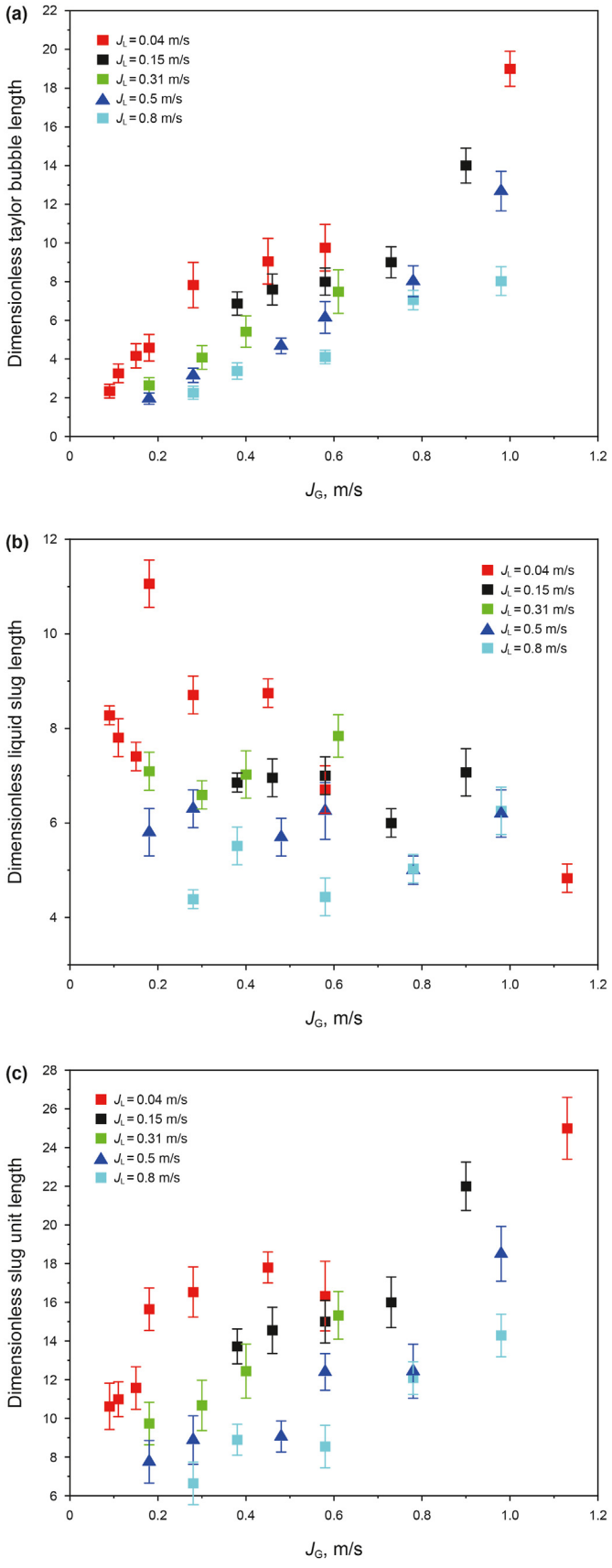

Fig. 18. Dimensionless lengths of Taylor bubble, liquid slug and slug unit variation with J_G.

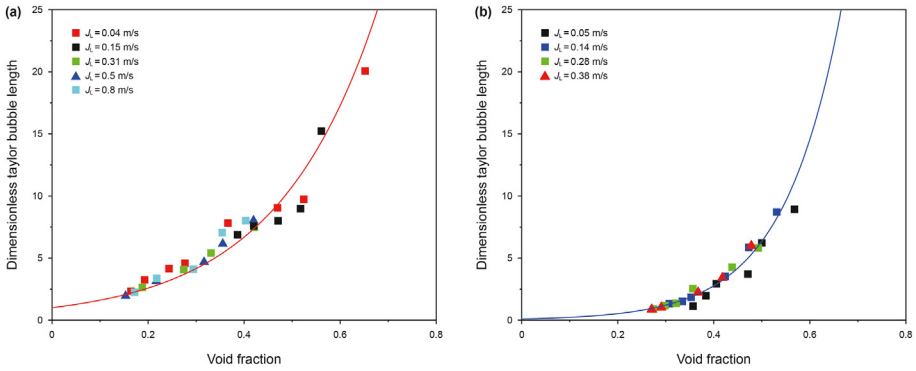

Fig. 19. The dimensionless Taylor bubble length as a function of void fraction, data from this paper and Abdulkadir et al., (2014).

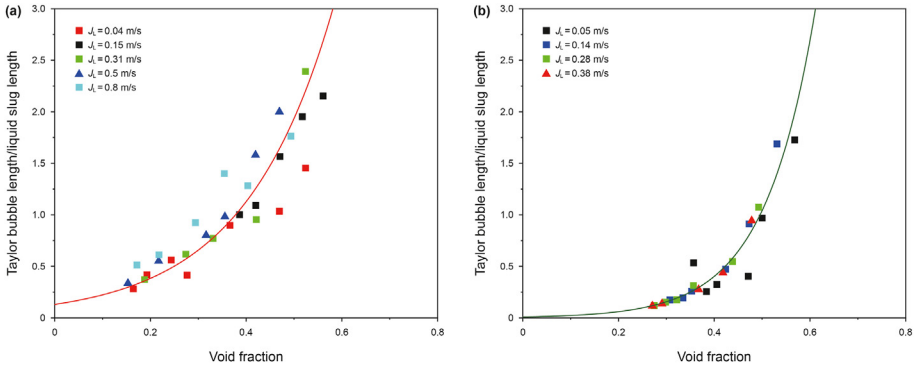

Fig. 20. Taylor bubble length to liquid slug length variation with void fraction, data from this paper and Abdulkadir et al., (2014).

According to Eqs. (23)–(27), dimensionless lengths of Taylor bubble (L_{TB}/D), liquid slug (L_S/D) and slug unit (L_{SU}/D) variation with gas superficial velocity were plotted and shown in Fig. 18. Increasing gas superficial velocity will enhance the coalescence probability between bubbles in liquid and lead to the growth of bubbles under a constant liquid superficial velocity. Therefore, Taylor bubble lengths show the approximately linear increase as gas superficial velocity increases. Under the same gas superficial velocity, increasing liquid superficial velocity will trigger unstable fluctuation of liquid film around Taylor bubbles, which will increase the amount of liquid entrained into bubbles and lead to the deformation and rupture of Taylor bubbles. Thus, Fig. 18(a) shows the lengths of Taylor bubble decrease as the liquid superficial velocity increases.

In Fig. 18(b), liquid slug lengths don't manifest systematic trend, which was also found in Abdulkadir's experiment. Experimental studies by scholars (Van Hout et al., 2002) found that lengths of liquid slug were stable between 8 and 25D. Their research is based on small vertical pipes, whose wall has a strong bondage effect on the phase interface and make liquid slug easier to maintain stability. Therefore, the liquid slug length range is larger than that obtained in the medium vertical pipe (4–12D).

The slug unit is determined by the Taylor bubble and liquid slug together. Therefore, the slug unit lengths don't show the obvious linear ascendent trends as gas superficial velocity increases, as shown in Fig. 18(c). Nevertheless, Taylor bubble growth still plays a dominant role in the growth of slug unit length.

4.5.2. Slug unit structure variation with void fraction

Other scholars (Kaji et al., 2009; Abdulkadir et al., 2014) also found the similar distribution of slug structure described above. However, they did not explore the distribution of Taylor bubble length as a function of void fraction. Therefore, this paper explores the influence of void fraction on the Taylor bubble.

Fig. 19(a) shows the curve of the Taylor bubble dimensionless length variation with void fraction. Taylor bubble length shows an exponentially ascendant tendency as void fraction increases under different liquid superficial velocities. Abdulkadir's experimental data were analyzed and the same distribution trend was found, as shown in Fig. 19(b). It manifests that the Taylor bubble lengths in pipes are an exponential function of void fraction, namely $L_{TB} = f\times[A\times\mathrm{EXP}(B\times\varepsilon_g)]$. Nevertheless, there are less systematic variations of liquid slug length and slug unit length with void fraction.

It is important to study Taylor bubble length to liquid slug length in analyzing void fraction of slug structure. According to the slug unit composition, the liquid slug length L_S can be determined as follows:

$$L_S = \frac{\varepsilon_g - \varepsilon_{TB}}{\varepsilon_{gs} - \varepsilon_{TB}} L_{SU} \tag{28}$$

According to $L_{SU} = L_{TB} + L_S$, change the form of Eq. (28) and get:

$$\frac{L_{TB}}{L_S} = \frac{\varepsilon_g - \varepsilon_{gs}}{\varepsilon_{TB} - \varepsilon_g} \tag{29}$$

where ε_g, ε_{TB} and ε_{gs} represent the average void fraction in slug unit (α in this paper), Taylor bubble and liquid slug, respectively. Fig. 20(a) shows the ratio of Taylor bubble length to liquid slug length increases exponentially with void fraction increasing. Data of Abdulkadir experiment were processed and then plotted in Fig. 20(b). It indicates that Taylor bubble length to liquid slug length exponential variation with the void fraction, namely $L_{TB}/L_S = f\times$

$[C\times\mathrm{EXP}(D\times\varepsilon_g)]$. A large number of scholars have studied void fraction in different components of slug unit but there is no universal conclusion. It is found that Taylor bubble length and the ratio of Taylor bubble length to liquid slug length are exponential functions of void fraction, namely $L_{TB} = f\times[A\times\mathrm{EXP}(\mathrm{B}\times\varepsilon_g)]$, $L_{TB}/L_S = f\times[C\times\mathrm{EXP}(D\times\varepsilon_g)]$. Under the condition that ε_g, $L_{TB} = f\times[A\times\mathrm{EXP}(\mathrm{B}\times\varepsilon_g)]$ and $L_{TB}/L_S = f\times[C\times\mathrm{EXP}(D\times\varepsilon_g)]$ are known, the proportional relationship between ε_{TB} and ε_{gs} can be determined. This finding provides a new idea for investigating the void fraction in Taylor bubble and liquid slug and which can be used in calculating two-phase flow density and improving the hydrodynamic model.

5. Conclusions

The visual experimental investigation on air-water flow was carried out in a vertical pipe with the 80 mm diameter and 11 m height. The gas superficial velocity and liquid superficial velocity are from 0.03 to 16 m/s and 0.04–2 m/s. A flow regime map was drawn on the basis of image data obtained from a high-speed camera. Void fraction in different working conditions was analyzed by the method of Power Spectrum Density (PSD) and the evolution of slug frequency was studied. Main conclusions are as follows.

(1) Flow maps of 50–189 mm diameters vertical pipes were compared and the influence of pipe diameters on flow regime transitions was analyzed. when D was larger than 80 mm, the transition boundary from bubble to slug flow moved to a larger gas velocity with the increase of diameters. Models proposed by Lucas and Taitel had high accuracy in predicting transitions from bubble to slug flow and churn to annular flow, respectively.
(2) Drift-flux models were established in different flow regions and liquid properties had significant effect on drift coefficients of bubble flow and slug flow (void fraction $\alpha \leq 0.4$). However, the effect of liquid properties is obviously weakened due to rapid and uniform mixing of gas and liquid in churn flow. Several drift-flux models were compared, among which the Nicklin's model had the smallest prediction deviation (7.5%).
(3) Void fraction along with the pipeline was compared. The turbulence effect caused by high gas velocity would induce a significant increase in the void fraction at inlet, whose influence would move to low gas velocities (11, 8 and 5 m/s) with the increase of liquid velocities (0.31, 0.5 and 0.8 m/s). At 85D from the vertical pipe base, the influence of inlet effect on the gas-liquid interface disappeared and where flow was fully developed.
(4) According to the phenomenon that the slug frequency increased first and then decreased as gas Weber numbers increased at $J_L < 0.31$ m/s, a new slug frequency correlation was proposed. The ratio of Taylor bubble length to liquid slug length (L_{TB}/L_S) varied exponentially with void fraction.

Declaration of competing interest

The authors declare that they have no known competing financial interests or personal relationships that could have appeared to influence the work reported in this paper.

Acknowledgement

This work was supported by the National Natural Science Foundation of China (No. 51888103, No. 52076175.

Nomenclature

A	pipe cross area, m^2
J_G	gas superficial velocity, m/s
J_L	liqiud superficial velocity, m/s
J	mixture velocity, m/s
U_g	gas velocity, m/s
C_0	distribution parameter
k	drift coefficient
V_{gi}	drift velocity, m/s
L	distance from the pipe inlet, m
D	pipe diameter, m
L_{TB}	Taylor bubble length, m
L_S	liquid slug length, m
L_{SU}	slug unit length, m
g	gravitation, m/s^2

Greek symbols

α	void fraction
μ	viscosity, mPa·s
ρ	density, kg/m^3
σ	surface tension, N/m
ε_{gs}	void fraction in liquid slug
ε_{TB}	void fraction in Taylor bubble
ε_g	void fraction in slug unit (α)

Non-dimensional numbers

W_E	$= \rho_G J_G^2 D/\sigma$
R_{eL}	$= \rho_L J_L D/\mu_L$
$D_H{}^*$	$= D_H\sqrt{\sigma/g\Delta\rho}$

References

Abdulkadir, M., Hernandez-Perez, V., Kwatia, C.A., et al., 2018. Interrogating flow development and phase distribution in vertical and horizontal pipes using advanced instrumentation. Chem. Eng. Sci. 186, 152–167. https://doi.org/10.1016/j.ces.2018.04.039.

Abdulkadir, M., Hernandez-Perez, V., Lowndes, I.S., et al., 2014. Detailed analysis of phase distributions in a vertical riser using wire mesh sensor (WMS). Exp. Therm. Fluid Sci. 59, 32–42. https://doi.org/10.1016/j.expthermflusci.2014.07.010.

Abdulkadir, M., Ugwoke, B., Abdulkareem, L., et al., 2021. Experimental investigation of the characteristics of the transition from spherical cap bubble to slug flow in a vertical pipe. Exp. Therm. Fluid Sci. 124, 110349. https://doi.org/10.1016/j.expthermflusci.2021.110349.

Ali, S.F., 2009. Two-phase Flow in a Large Diameter Vertical Riser. Cranfield University.

Amani, P., Hurter, S., Rudolph, V., et al., 2020. Comparison of flow dynamics of air-water flows with foam flows in vertical pipes. Exp. Therm. Fluid Sci. 119, 110216. https://doi.org/10.1016/j.expthermflusci.2020.110216.

Arabi, A., Ragui, K., Salhi, Y., et al., 2020. Slug frequency for a gas-liquid plug flow: review and development of a new correlation. Int. Commun. Heat Mass Tran. 118. https://doi.org/10.1016/j.icheatmasstransfer.2020.104841.

Baba, Y.D., Aliyu, A.M., Archibong, A.E., et al., 2018. Slug length for high viscosity oil-gas flow in horizontal pipes: experiments and prediction. J. Petrol. Sci. Eng. 165, 397–411. https://doi.org/10.1016/j.petrol.2018.02.003.

Barnea, D., Luninski, Y., Taitel, Y., 1983. Flow pattern in horizontal and vertical two phase flow in small diameter pipes. Can. J. Chem. Eng. 61. https://doi.org/10.1002/cjce.5450610501.

Gao, X.F., Xie, W.D., Hai, X.W., 2020. Vortex-Induced vibrations of A free-spanning pipe based on A nonlinear hysteretic soil model at the shoulders. China Ocean Eng. 34, 328–340. https://doi.org/10.1007/s13344-020-0030-8.

Gregory, G., Scott, D., 1969. Correlation of liquid slug velocity and frequency in horizontal cocurrent gas-liquid slug flow. AIChE J. 15, 933–935. https://doi.org/10.1002/aic.690150623.

Gu, J.Y., Xie, Y.L., Zhao, Y., et al., 2018. Study on vortex-induced motions of A new type of deep draft multi-columns FDPSO. China Ocean Eng. 32, 1–13. https://doi.org/10.1007/s13344-018-0001-5.

Gui, M., Liu, Z., Liao, B., et al., 2019. Void fraction measurements of steam–water two-phase flow in vertical rod bundle: comparison among different techniques. Exp. Therm. Fluid Sci. 109, 109881. https://doi.org/10.1016/j.expthermflusci.2019.109881.

Hernandez-Perez, V., Abdulkadir, M., Azzopardi, B., 2010. Slugging frequency correlation for inclined gas-liquid flow. World Academy of Science. Eng. Technol. 37.

Hibiki, T., Ishii, M., 2003. One-dimensional drift-flux model and constitutive equations for relative motion between phases in various two-phase flow regimes. Int. J. Heat Mass Tran. 46, 4935–4948. https://doi.org/10.1016/S0017-9310(03)00322-3.

Hong, B.Y., Liu, S.N., Li, X.P., et al., 2022. A liquid loading prediction method of gas pipeline based on machine learning. Petrol. Sci. https://doi.org/10.1016/j.petsci.2022.05.002.

Isao, K., Mamoru, I., 1987. Drift flux model for large diameter pipe and new correlation for pool void fraction. Int. J. Heat Mass Tran. 30, 1927–1939. https://doi.org/10.1016/0017-9310(87)90251-1.

Jepson, W., Taylor, R., 1993. Slug flow and its transitions in large-diameter horizontal pipes. Int. J. Multiphas. Flow 19, 411–420. https://doi.org/10.1016/0301-9322(93)90057-2.

Ju, G.S., Yan, T., Sun, X.F., et al., 2022. Evolution of gas kick and overflow in wellbore and formation pressure inversion method under the condition of failure in well shut-in during a blowout. Petrol. Sci. 19, 678–687. https://doi.org/10.1016/j.petsci.2022.01.004.

Kaichiro, M., Ishii, M., 1984. Flow regime transition criteria for upward two-phase flow in vertical tubes. Int. J. Heat Mass Tran. 27, 723–737. https://doi.org/10.1016/0017-9310(84)90142-X.

Kaji, R., Azzopardi, B.J., Lucas, D., 2009. Investigation of flow development of co-current gas-liquid vertical slug flow. Int. J. Multiphas. Flow 35, 335–348. https://doi.org/10.1016/j.ijmultiphaseflow.2009.01.004.

Kawanishi, K., Hirao, Y., Tsuge, A., 1990. An experimental study on drift flux parameters for two-phase flow in vertical round tubes. Nucl. Eng. Des. 120, 447–458. https://doi.org/10.1016/0029-5493(90)90394-D.

Legius, H.J.W.M., Vandenakker, H.E.A., Narumo, T., 1997. Measurements on wave propagation and bubble and slug velocities in cocurrent upward two-phase flow. Exp. Therm. Fluid Sci. 15, 267–278. https://doi.org/10.1016/S0894-1777(97)00012-5.

Liu, W., Xu, Q., Zou, S., et al., 2021. Optimization of differential pressure signal acquisition for recognition of gas–liquid two-phase flow patterns in pipeline-riser system. Chem. Eng. Sci. 229, 116043. https://doi.org/10.1016/j.ces.2020.116043.

Lucas, D., Krepper, E., Prasser, H.M., 2005. Development of co-current air–water flow in a vertical pipe. Int. J. Multiphas. Flow 31, 1304–1328. https://doi.org/10.1016/j.ijmultiphaseflow.2005.07.004.

Naidek, B.P., Conte, M.G., Cozin, C., et al., 2022. Experimental study of influence of liquid viscosity in horizontal slug flow. Exp. Therm. Fluid Sci. https://doi.org/10.1016/j.expthermflusci.2022.110798.

Nicklin, D., 1962. Two-phase bubble flow. Chem. Eng. Sci. 17, 693–702. https://doi.org/10.1016/0009-2509(62)85027-1.

Omebere-Iyari, N.K., Azzopardi, B.J., Lucas, D., et al., 2008. The characteristics of gas/liquid flow in large risers at high pressures. Int. J. Multiphas. Flow 34, 461–476. https://doi.org/10.1016/j.ijmultiphaseflow.2007.11.001.

Oshinowo, T., Charles, M., 1974. Vertical two-phase flow: Part II. Holdup and pressure drop. Can. J. Chem. Eng. 52, 438–448. https://doi.org/10.1002/cjce.5450520402.

Rodrigues, R.L., Cozin, C., Naidek, B.P., et al., 2020. Statistical features of the flow evolution in horizontal liquid-gas slug flow. Exp. Therm. Fluid Sci. 119, 110203. https://doi.org/10.1016/j.expthermflusci.2020.110203.

Schlegel, J.P., Sawant, P., Paranjape, S., et al., 2009. Void fraction and flow regime in adiabatic upward two-phase flow in large diameter vertical pipes. Nucl. Eng. Des. 239, 2864–2874. https://doi.org/10.1016/j.nucengdes.2009.08.004.

Sekhavati, J., Hashemabadi, S.H., Soroush, M., 2022. Computational methods for pipeline leakage detection and localization: a review and comparative study. J. Loss Prev. Process. Ind. 77. https://doi.org/10.1016/j.jlp.2022.104771.

Shoukri, M., Tawfik, H., Chan, A.M.C., 1984. 2-phase redistribution in horizontal subchannel flow turbulent mixing and gravity separation. Int. J. Multiphas. Flow 10, 357–369. https://doi.org/10.1016/0301-9322(84)90026-0.

Smith, T.R., Schlegel, J.P., Hibiki, T., et al., 2012. Two-phase flow structure in large diameter pipes. Int. J. Heat Fluid Flow 33, 156–167. https://doi.org/10.1016/j.ijheatfluidflow.2011.10.008.

Szalinski, L., Abdulkareem, L.A., Da Silva, M.J., et al., 2010. Comparative study of gas–oil and gas–water two-phase flow in a vertical pipe. Chem. Eng. Sci. 65, 3836–3848. https://doi.org/10.1016/j.ces.2010.03.024.

Taitel, Y., Bornea, D., Dukler, A.E., 1980. Modeling flow pattern transitions for steady upward gas-liquid flow in vertical tubes. AIChE J. 26, 345–354. https://doi.org/10.1002/aic.690260304.

Tas-Koehler, S., Neumann-Kipping, M., Liao, Y., et al., 2022. Experimental investigations and numerical assessment of liquid velocity profiles and turbulence for single- and two-phase flow in a constricted vertical pipe. Int. J. Multiphas. Flow 157. https://doi.org/10.1016/j.ijmultiphaseflow.2022.104224.

Tengesdal, J., Kaya, A.S., Sarica, C., 1999. Flow-pattern transition and hydrodynamic modeling of churn flow. SPE J. 4. https://doi.org/10.2118/57756-PA.

Van Hout, R., Gulitski, A., Barnea, D., et al., 2002. Experimental investigation of the velocity field induced by a Taylor bubble rising in stagnant water. Int. J. Multiphas. Flow 28, 579–596. https://doi.org/10.1016/S0301-9322(01)00082-9.

Wang, D., Jin, N., Zhai, L., et al., 2022. Quantitative research of the liquid film characteristics in upward vertical gas, oil and water flows. Chin. J. Chem. Eng. https://doi.org/10.1016/j.cjche.2022.03.004.

Wang, T., Gui, M., Zhao, J., et al., 2021. Void fraction measurement and calculation model of. vertical upward co-current air–water slug flow. Chin. J. Chem. Eng. https://doi.org/10.1016/j.cjche.2021.10.003.

Wang, X., Sun, J., Zhao, J., et al., 2017. Experimental detection of bubble-wall interactions in a vertical gas–liquid flow. Chin. J. Chem. Eng. 25, 838–847. https://doi.org/10.1016/j.cjche.2016.11.013.

Wang, Y., Li, P., Liu, Y., et al., 2022. Experimental study on vortex-induced vibration coupling wake inter-ference of multi-riser groups with sensitive spacing. China Ocean Eng. 36, 333–347. https://doi.org/10.1007/s13344-022-0030-y.

Wang, Z., He, Y., Li, M.Z., et al., 2021. Fluid-structure interaction of two-phase flow passing through 90° pipe bend under slug pattern conditions. China Ocean Eng. 35, 914–923. https://doi.org/10.1007/s13344-021-0080-6.

Wang, Z., Kang, Y., Wang, X., et al., 2018. Investigation of the hydrodynamics of slug flow in airlift pumps. Chin. J. Chem. Eng. 26, 2391–2402. https://doi.org/10.1016/j.cjche.2018.04.015.

Wang, Z.N., Kang, Y., Wang, X.C., et al., 2018. Investigating the flow characteristics of air-lift pumps operating in gas-liquid two-phase flow. Chin. J. Chem. Eng. 26, 219–227. https://doi.org/10.1016/j.cjche.2017.09.011.

Wu, B., Firouzi, M., Mitchell, T., et al., 2017. A critical review of flow maps for gas-liquid flows in vertical pipes and annuli. Chem. Eng. J. 326, 350–377. https://doi.org/10.1016/j.cej.2017.05.135.

Xie, W., Xu, W.H., Zhai, L., et al., 2019. Dynamic behaviors of A marine riser under two different frequency parametric excitations. China Ocean Eng. 33, 704–712. https://doi.org/10.1007/s13344-019-0068-7,ISSN0890-5487.

Xu, Q., Liu, C., Liu, Q., et al., 2022. Interfacial characteristics of steam jet condensation in subcooled water pipe flow–An experimental and numerical study. Chem. Eng. Sci. 251, 117457. https://doi.org/10.1016/j.ces.2022.117457.

Xu, Q., Liu, C., Wang, X., et al., 2021. Machine learning classification of flow regimes in a long pipeline-riser system with differential pressure signal. Chem. Eng. Sci. 233, 116402. https://doi.org/10.1016/j.ces.2020.116402.

Xu, Q., Wang, X., Chang, L., et al., 2022. Signal optimization for recognition of gas–liquid two-phase flow regimes in a long pipeline-riser system. Measurement 200, 111581. https://doi.org/10.1016/j.measurement.2022.111581.

Xu, Q., Wang, X., Luo, X., et al., 2022. Machine learning identification of multiphase flow regimes in a long pipeline-riser system. Flow Meas. Instrum. 88, 102233. https://doi.org/10.1016/j.flowmeasinst.2022.102233.

Xu, Q., Zhu, Y., Zhou, H., et al., 2022. Flow characteristic of steam jet condensed into a water pipe flow-a numerical study. Appl. Therm. Eng. 205, 118034. https://doi.org/10.1016/j.applthermaleng.2022.118034.

Xu, Z., Hu, T., Pang, X.Q., et al., 2022. Research progress and challenges of natural gas hydrate resource evaluation in the South China Sea. Petrol. Sci. 19, 13–25. https://doi.org/10.1016/j.petsci.2021.12.007.

Yin, B.T., Li, X.F., Liu, G., 2018. A mechanistic model of heat transfer for gas-liquid flow in vertical wellbore annuli. Petrol. Sci. 15, 135–145. https://doi.org/10.1007/s12182-017-0193-y.

Zhang, H., Lan, H.Q., 2017. A review of internal corrosion mechanism and experimental study for pipelines based on multiphase flow. Corrosion Rev. 35, 425–444. https://doi.org/10.1016/j.applthermaleng.2022.118034.

Zuber, N., Findlay, J., 1965. Average volumetric concentration in two-phase flow systems. J. Heat Tran. 87, 4. https://doi.org/10.1115/1.3689137.